Title

Nanoparticle Formulation of Moxifloxacin and Intramuscular Route of Delivery Improve Antibiotic Pharmacokinetics and Treatment of Pneumonic Tularemia in a Mouse Model

Journal

ACS Infectious Diseases, 5(2)

ISSN

2373-8227

Authors

Clemens, Daniel L
Lee, Bai-Yu
Plamthottam, Sheba
et al.

Publication Date

2019-02-08

DOI

10.1021/acsinfecdis.8b00268

Nanoparticle formulation of moxifloxacin and intramuscular route of delivery improve antibiotic pharmacokinetics and treatment of pneumonic tularemia in a mouse model

Journal:	*ACS Infectious Diseases*
Manuscript ID	id-2018-002684.R1
Manuscript Type:	Article
Date Submitted by the Author:	n/a
Complete List of Authors:	Clemens, Daniel; University of California Los Angeles, Department of Medicine Lee, Bai-Yu; University of California Los Angeles, Medicine Plamthottam, Sheba; UCLA Division of Physical Sciences, Chemistry Tullius, Michael; University of California, Los Angeles Wang, Ruining; University of California, Los Angeles, Department of Chemistry and Biochemistry Yu, Chia-Jung; University of California, Los Angeles, Department of Chemistry and Biochemistry Li, Zilu; PPG Industries Inc, Coating Innovation Center Dillon, Barbara; University of California, Los Angeles, Department of Medicine Zink, Jeffrey; University of California Los Angeles, Chemistry and Biochemistry Horwitz, Marcus; University of California Los Angeles, Medicine

Nanoparticle formulation of moxifloxacin and intramuscular route of delivery improve antibiotic pharmacokinetics and treatment of pneumonic tularemia in a mouse model

Daniel L. Clemens[a], Bai-Yu Lee[a], Sheba Plamthottam[b]. Michael V. Tullius[a], Ruining Wang[b], Chia-Jung Yu[b], Zilu Li[b], Barbara Jane Dillon[a], Jeffrey I. Zink[b,c], and Marcus A. Horwitz[a,*]

[a]Division of Infectious Diseases, Department of Medicine, University of California Los Angeles, CHS 37-121, 10833 Le Conte Ave., CA 90095-1688, USA

[b]Department of Chemistry and Biochemistry, University of California, Los Angeles, 3013 Young Dr. East, CA 90095-1569, USA

[c]California NanoSystems Institute, University of California, Los Angeles, CA 90095-8352, USA

*Corresponding author: Marcus A. Horwitz, Division of Infectious Diseases, Department of Medicine, UCLA School of Medicine, CHS 37-121, 10833 LeConte Avenue, Los Angeles, CA 90095-1688; Phone: 310-206-0074; Fax: 310-794-7156; E-mail: mhorwitz@mednet.ucla.edu

Francisella tularensis causes a serious and often fatal infection, tularemia. We compared the efficacy of moxifloxacin formulated as free drug vs. disulfide snap-top mesoporous silica nanoparticles (MSNs) in a mouse model of pneumonic tularemia. We found that MSN-formulated moxifloxacin was more effective than free drug and that the intramuscular and subcutaneous routes were markedly more effective than the intravenous route. Measurement of tissue silica levels and fluorescent flow cytometry assessment of colocalization of MSNs with infected cells revealed that the enhanced efficacy of MSNs and the intramuscular route of delivery was not due to better delivery of MSNs to infected tissues or cells. However, moxifloxacin blood levels demonstrated that the nanoparticle formulation and intramuscular route provided the longest half-life and longest time above the minimal inhibitory concentration. Thus, improved pharmacokinetics are responsible for the greater efficacy of nanoparticle formulation and intramuscular delivery compared with free drug and intravenous delivery.

Keywords: Mesoporous Silica Nanoparticles, Pharmacokinetics, Moxifloxacin, Tularemia, Francisella tularensis, Nanotherapeutics

Mesoporous silica nanoparticles (MSNs) are an attractive drug delivery platform for several reasons, including an extremely large internal surface area that allows high drug loading and a surface that can be readily modified for targeting of specific cells and controlled drug release in response to environmental cues.[1,2] For example, we have devised MSNs functionalized with disulfide snap-tops that release their drug cargo intracellularly in response to the intracellular redox potential.[3,4] We have previously shown that intravenous (i.v.) administration of moxifloxacin (MXF) via disulfide snap-top redox-operated MSNs (MSN-SS-MXF) is much more effective for treatment of pneumonic tularemia in mice than an equivalent amount of free drug[3] (i.e. non-MSN encapsulated drug). However, the basis for the enhanced efficacy was not determined. Nanoparticle (NP)-delivered antibiotics have been proposed to have numerous advantages over free drugs, including shielding the drug from excretion and metabolism, improved pharmacokinetics,[5] and specific targeting of macrophages in the lung and reticuloendothelial system, which are important host cells for intracellular pathogens, such as *Francisella* tularensis[3,6] and *Mycobacterium* tuberculosis.[7] The relative contribution of various factors to the enhanced efficacy of MSN-delivered drug vs. free drug is often unclear.

A study in *Mycobacterium marinum* infected zebrafish embryos demonstrated that poly(lactic-co-glycolic acid) (PLGA) NPs administered i.v. are taken up by macrophages that traffic into *M. marinum* containing granulomas,[8] consistent with the concept that a NP platform can enhance drug delivery to infected cells and tissues. However, the study did not examine whether i.v. administration of the PLGA-delivered drug was more effective than other routes, e.g. the subcutaneous (s.c.) or intramuscular (i.m.) route, where trafficking of NP-containing drug to the site of infection might be less effective.

Here we determined the efficacy of MSN-SS-MXF delivered i.v., s.c., or i.m. against lethal respiratory infection with *F. tularensis* subsp. *holarctica* Live Vaccine Strain (LVS) in mice. We show that equivalent amounts of MXF exhibit the following order of efficacy for treatment of pneumonic tularemia in a mouse model: i.m. MSN-SS-MXF > i.v. MSN-SS-MXF > i.m. free MXF > i.v. free MXF. We conducted additional studies to determine whether the improved efficacy of the MSN formulation and the i.m. route of administration was attributable to improved delivery to infected cells or to improved pharmacokinetics. While i.m. administered MSN-SS-MXF was the most effective, we found few or no MSNs in the lungs of mice following i.m. administration, indicating that, for this NP platform, enhanced trafficking of MSN-SS-MXF to the site of infection is not responsible for the markedly enhanced efficacy of the i.m. route. On the other hand, the nanoparticle formulation yields a longer half-life than free drug and i.m. administration yields an even further prolongation of the half-life. In our model of pneumonic tularemia, time above the minimal inhibitory concentration (t>MIC) is the best predictor of MXF efficacy, and accordingly, i.m. administration of the nanoparticle formulation of MXF was superior to all other routes and to free MXF.

RESULTS

Characterization of properties of MSN-SS-MXF

We examined the MSN by transmission electron microscopy (TEM) before (Fig. 1A-B) and after surface modification for incorporation of the snap-top nanovalves (Fig. 1C-D) and observed that the MSN were well dispersed and of uniform size. Dynamic light scattering (DLS) measurement of the MSN-SS-MXF showed them to have a mean hydrodynamic diameter of 182 nm. The MSN-SS-MXF exhibited a zeta potential of -30 mV in deionized water. The MSN-SS-MXF showed a total loading of 35.9% MXF (wt/wt %), comprising 2.3% residual drug and a specific release (with DMSO and 2-mercaptoethanol reducing agent) of 33.6%. These properties are very similar to those which we have observed previously for these nanoparticles.[3]

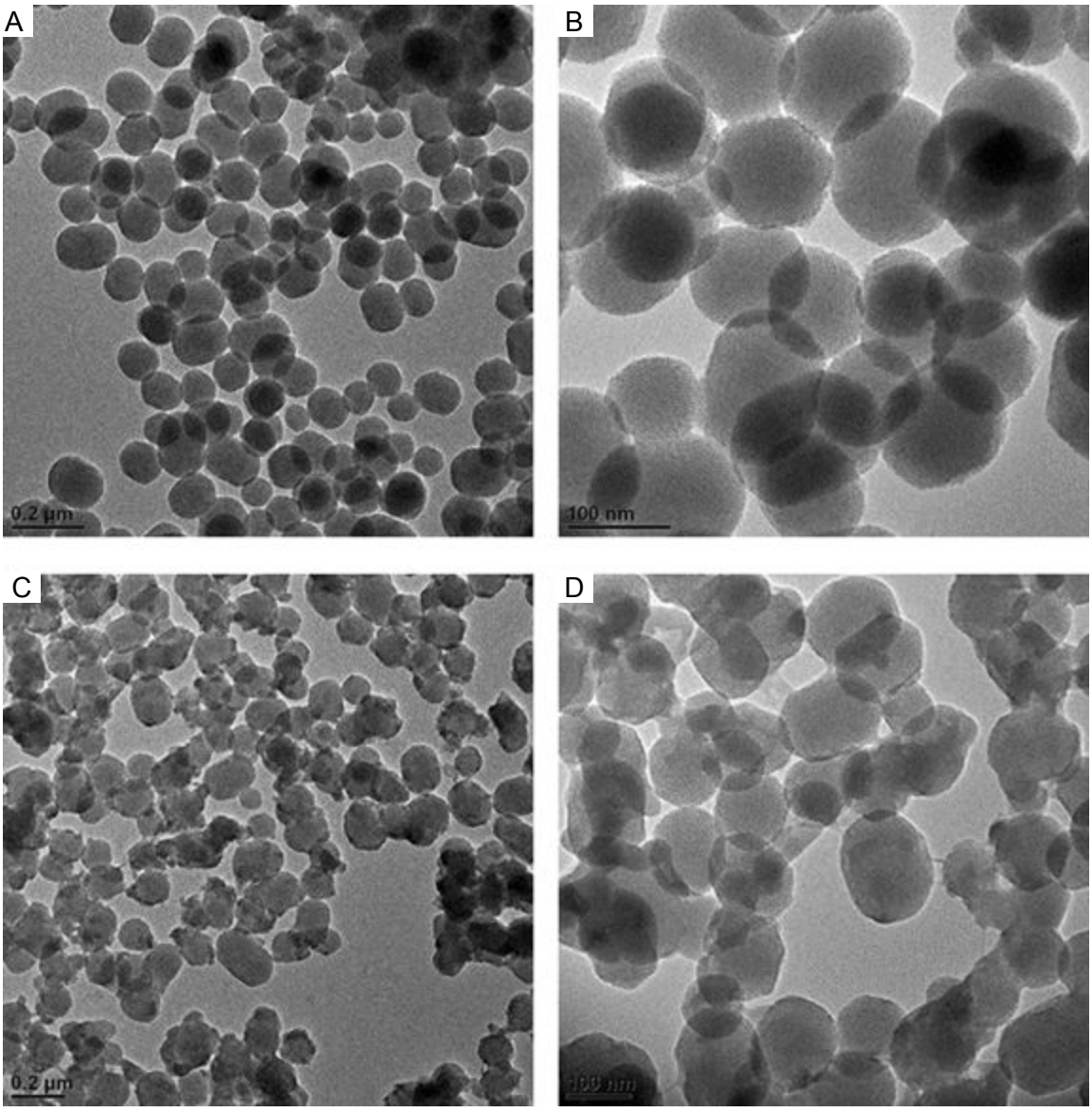

Fig. 1. TEM image of MSN before (A - B) and after (C - D) surface modification to incorporate redox-operated snap-top nanovalves. Size bars (A, C) 0.2 µm; (B, D) 100 nm.

Efficacy of MSN-SS-MXF and free MXF by 3 different routes of administration

We conducted two independent experiments to compare the treatment efficacy of MSN-SS-MXF delivered via three different routes in a mouse model of pneumonic tularemia. We infected BALB/c mice intranasally (i.n.) with 6 times the LD_{50} of *F. tularensis* LVS and one day later

began treatment by the i.v., i.m., or s.c. routes with either free MXF (50 – 200 μg) or MSN-SS-MXF encapsulated MXF. In the first experiment, the MSN-SS-MXF encapsulated MXF was given at a dose of 60 μg of MXF (Fig. 2A) and in the second experiment the MSN-SS-MXF was given at doses of 50 and 100 μg MXF (Fig. 2B). Doses were given every 48 hours for a total of 3 doses. We have found in a previous study that this dosing is optimal in assessing efficacy of free vs. nanoparticle formulated MXF by intravenous administration in a mouse model of pneumonic tularemia.[3] Higher doses or more frequent administration causes an efficacy plateau (unmeasurable organ burden) precluding comparisons of treatment efficacy.

In the first experiment, the number of live LVS [colony-forming units (CFU)] in the lung at 5 hours post-infection was determined to be 2.7×10^2 per lung. One day later, the bacterial burden increased to 1.4×10^5 CFU per lung. Without treatment, the bacteria continued to multiply in the lung and disseminate to other organs. At the end of the 6-day infection period, the bacterial number had multiplied to more than 10^7 CFU in the lung and $10^6 – 10^7$ CFU in the liver and spleen (Figure 2A).

In the first experiment, MSN-SS-MXF (60 μg) given by the i.m. route showed efficacy in reducing bacterial burden in the lungs comparable to that of a 3.3-fold larger dose (200 μg) of free drug given by the same i.m. route. MSN-SS-MXF was also more effective by the i.m. route than the s.c. or i.v. routes. By the s.c. route, MSN-SS-MXF (60 μg) was more effective than 100 μg of free MXF, and by the i.v. route, the efficacy of MSN-SS-MXF (60 μg) was comparable to that of 100 μg of free MXF. In the liver, i.m. MSN-SS-MXF (60 μg) was more effective than 100 μg of free MXF given i.m. and was more effective than MSN-SS-MXF (60 μg) given i.v. or

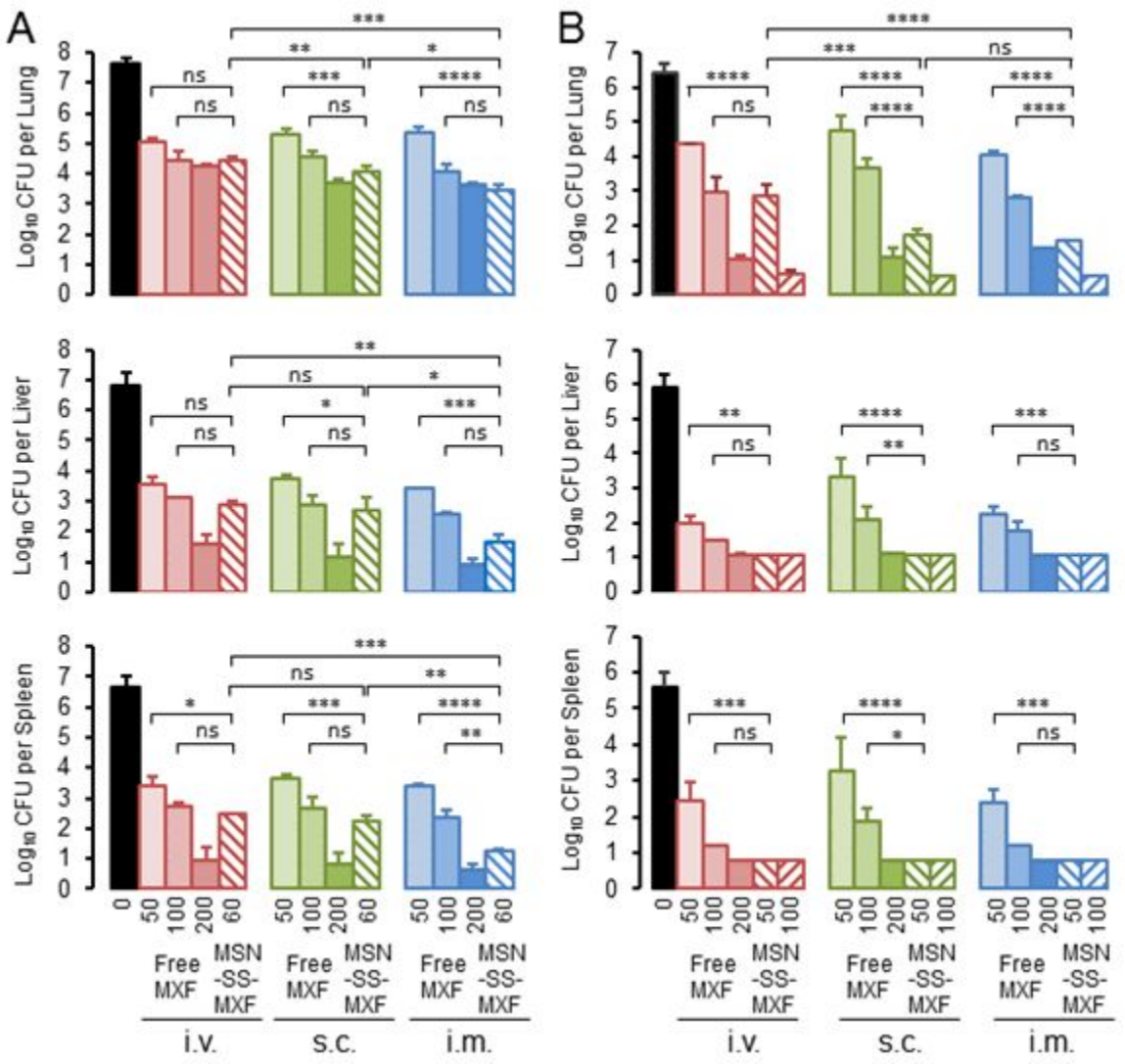

Fig. 2. Efficacy of MSN-SS-MXF and free MXF administered i.v., s.c., or i.m. in two independent experiments. BALB/c mice were infected with *F. tularensis* LVS i.n. at day 0. Mice were treated on day 1, 3, and 5 with free MXF (n = 3 mice/group) or MSN-SS-MXF (n = 4 mice/group) at the dose and route of administration indicated. Control mice were sham-treated with PBS i.v. Doses of MSN-SS-MXF indicated in the first (A) and second (B) experiments were the amount of free MXF-equivalent delivered. Bacterial burdens in the lung (top panel), liver (middle panel), and spleen (bottom panel) were determined one day after the last treatment

on day 6. Data are mean ± SEM. Treatment efficacy between groups was analyzed using two-way ANOVA with Tukey's multiple comparisons test. ****, $p < 0.0001$; ***, $p < 0.001$; **, $p < 0.01$; *, $p < 0.05$; ns, not significant

s.c. MSN-SS-MXF (60 μg) given i.m. reduced bacterial burden in the spleen to a greater extent than 100 μg of free MXF by the same route. MSN-SS-MXF (60 μg) given i.v. or s.c. also decreased bacterial burden to a greater extent than 100 μg of free MXF by the same routes.

In the second experiment, the number of bacteria in the lung at 5-hours and 1-day post infection was 1.5 x 10^2 CFU and 8 x 10^4 CFU, respectively. At day 6, the organ burden of bacteria was approximately 10^7 CFU in the lung and $10^5 – 10^6$ CFU in the liver and spleen (Figure 2B). Similar to the first experiment, MSN-SS-MXF (50 μg) given i.m. was as effective as a 4-fold higher dose (200 μg) of free MXF delivered by the same route in reducing bacterial burden in the lung. Also as observed in the first experiment, MSN-SS-MXF administered i.m. was more effective in reducing the lung bacterial load than equal amounts of MSN-SS-MXF given s.c. or i.v. In the liver and spleen, the effect of MSN-SS-MXF given by these three different routes could not be compared because bacterial number in these organs was reduced to a level below the experimental detection limit after treatment with three 50 μg doses, the lower of the two doses tested.

The design of these two experiments was the same except that, in the second experiment, to facilitate comparison of the different treatment methods, we included two concentrations of MSN-SS-MXF to match the lower (50 μg) and medium (100 μg) doses of free MXF. The infection dose was slightly different between the two studies, but within the range of variation commonly seen in this type of animal infection model. Nevertheless, both studies showed that

MSN-SS-MXF was more potent than free MXF and the drugs were more efficacious when given i.m. than i.v.

The median-effect equation[9,10] is widely used for modeling dose-response curves,[11-13] and we found that it accurately modeled our data. We used the median-effect equation to model the dose – response relationship between free MXF, administered by each of the routes, and reduction in bacterial burden in each of the organs, thereby allowing us to calculate – for each route and for each organ – the dose of free drug that would yield a comparable reduction in bacterial burden to MSN-delivered drug. We define the efficacy ratio as the ratio of the free drug to MSN-delivered drug that yields the same reduction in bacterial burden. Table 1 indicates the ratio of bio-equivalent amounts of MSN-SS-MXF to free MXF given by the same route. The efficacy ratios in the lung for MSN-SS-MXF vs. free MXF administered i.m., s.c., or i.v. were 2-3:1 in the first experiment and 3-4:1 in the second experiment (Table 1). The i.m. route had higher MSN-SS-MXF:free MXF efficacy ratios than s.c. and i.v. routes in liver and spleen in the first experiment and about the same efficacy ratios as s.c. and i.v. routes in the liver and spleen in the second experiment (Table 1); in the latter experiment, any potential improvements in the efficacy ratio by the i.m. route could not be ascertained because the efficacy of MSN-SS-MXF was already at a maximum, i.e., the bacterial burden in the liver and spleen - even with MSN-SS-MXF administered i.v. - was already reduced to the limit of detection (Fig. 2). Table 2 shows the ratio of the bio-equivalent amounts of MSN-SS-MXF and free MXF administered i.v., s.c., and i.m. relative to free MXF administered i.v. It is clear from Table 2 that MSN-SS-MXF are more efficacious than free drug by all routes of administration. Moreover, in the lung after administration of the 50 μg dose of MSN-SS-MXF, the only site and dose level where CFU were above the limit of detection, the i.m. and s.c. routes were more efficacious than the i.v. route.

Table 1. Efficacy ratios of MSN-SS-MXF:Free MXF

Experiment	Organ	MSN-SS-MXF Dose (μg)	Route of administration		
			i.v.	s.c.	i.m.
Experiment 1					
	Lung	60	2.10	2.40	3.36
	Liver	60	1.43	1.46	2.09
	Spleen	60	1.45	1.59	2.25
Experiment 2					
	Lung	50	1.84	3.28	3.58
		100	2.95	3.42	4.58
	Liver	50	4.19	4.19	4.11
		100	2.11	2.07	2.04
	Spleen	50	3.65	4.07	3.71
		100	1.84	2.02	1.88

Table 2. Efficacy ratios relative to i.v. free MXF in experiment 2

Treatment	Organ	MXF dose (μg)	Route of administration		
			i.v.	s.c.	i.m.
Free MXF	Lung	50	1.00	0.87	1.21
		100	1.00	0.69	0.94
		200	1.00	1.00	0.86
	Liver	50	1.00	0.19	0.69
		100	1.00	0.46	0.70
		200	1.00	0.95	1.09
	Spleen	50	1.00	0.49	0.98
		100	1.00	0.69	1.16
		200	1.00	0.90	0.89
MSN-SS-MXF	Lung	50	1.85	2.87	3.07
		100	2.86	3.09	3.17
	Liver	50	4.20	4.23	4.15
		100	2.11	2.06	2.06
	Spleen	50	3.57	3.61	3.57
		100	1.80	1.78	2.26

MXF formulated in nanoparticles and administered i.m. can act on *F. tularensis* at sites of infection by one of the following mechanisms: 1) nanoparticles injected into the muscle are taken up by macrophages and dendritic cells which then traffic via lymphatics and/or blood to infected organs where they release the MXF; 2) nanoparticles injected into the muscle travel freely via lymphatics or blood to infected organs, where the nanoparticles are taken up and release the MXF; or 3) nanoparticles injected into the muscle are taken up by cells in the muscle and free MXF is slowly released from muscle into the blood and circulates to the rest of the body. The i.m. route of administration generally confers a longer half-life than the i.v. route because the drug must transfer from the muscle into the systemic circulation before it can be cleared by hepatic or renal mechanisms. The nanoparticle formulation may have the advantage of conferring an even longer half-life by further prolonging the release of drug from the muscle. The third mechanism can be distinguished experimentally from the first two mechanisms by examining the lung and spleen tissue for silica and nanoparticles, since the first two mechanisms require that nanoparticles actually reach the infected organs after i.m. administration whereas the third mechanism does not.

Analysis of MSN silica in mouse organs by ICP-OES following i.m., s.c., and i.v. administration of MSN-SS-MXF

To determine whether greater delivery of MSNs to infected tissues could account for the greater efficacy of i.m. administration of MSN-SS-MXF, we measured MSN uptake into organs using inductively coupled plasma optical emission spectrometry (ICP-OES). Mice were given 3 doses, 48 hours apart, of MSN-SS-MXF i.v., s.c., or i.m. or 3 doses of PBS i.v., killed 24 hours after the

last injection, their organs digested with acid, and the amount of silica assayed by ICP-OES. We found that the level of silica per gram of tissue in the lung, liver, and spleen of mice treated with MSN-SS-MXF by i.m. or s.c. was comparable to the background level of silica in mice receiving sham (PBS) injections (Fig. 3). Only in mice treated with MSN-SS-MXF by the i.v. route were levels of silica in the organs greater than that in sham-treated mice (Fig. 3).

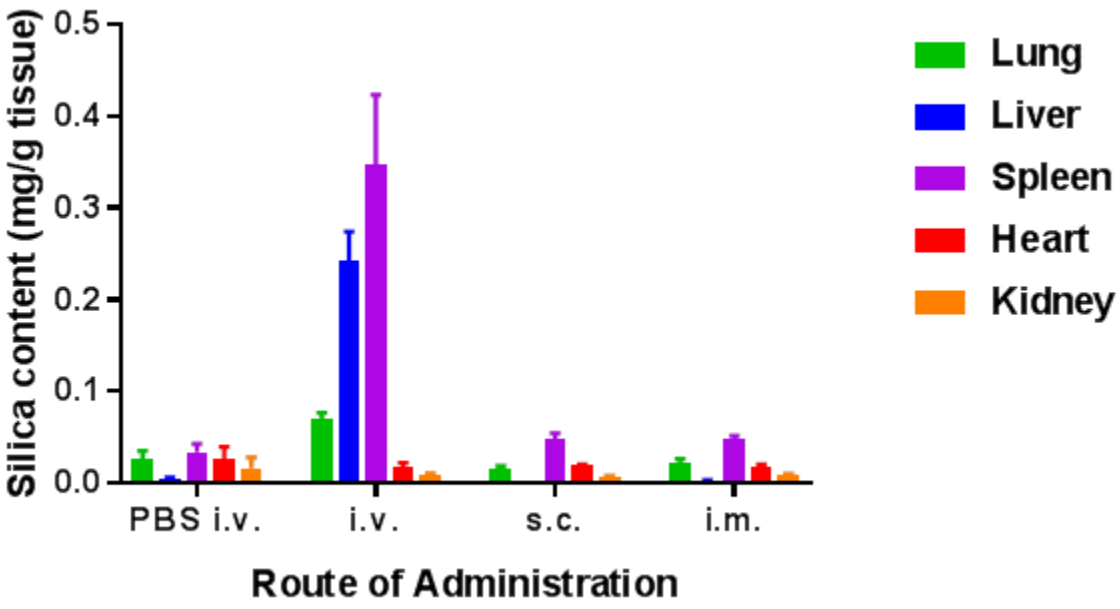

Fig. 3. Organ biodistribution of silica. The amount of silica in organs from *F. tularensis* LVS infected mice was determined after administration of MSN-SS-MXF via the route indicated. Data are mean ± SD of 3 mice in the PBS i.v. group and 4 mice each in the MSN-SS-MXF i.v., s.c., and i.m. groups.

Fluorescent MSNs are detected in the cells of infected organs after i.v. but not i.m. administration

To assess the trafficking of MSNs to infected cells and tissues, we infected mice i.n. with *F. tularensis* LVS that express GFP (LVS-GFP), and two days later injected DyLight 650-labeled MSNs into the mice by the i.v. and i.m. routes. One day after injection, the organs were digested enzymatically and by physical methods, immunostained with a fluorescent antibody to F4/80 (a mouse macrophage marker), and the cells examined with an ImageStream Mark II flow cytometer to assess co-localization of the MSNs and LVS-GFP. Whereas MSNs were present in infected F4/80+ macrophages of the lung and spleen (as well as F4/80- cells) following i.v. administration, they were not present in any cells (infected or uninfected) of these mouse organs after i.m. administration (Fig. 4). Thus, our flow cytometry findings (Fig. 4) were consistent with our ICP findings (Fig. 3); only i.v. administration of MSNs yielded detectable MSNs in the lung tissue, whereas i.m. administration did not. These results indicate that the MSN-SS-MXF do not travel to infected organs (lung, liver, or spleen) after i.m. admininstration, leaving only the pharmacokinetic explanation as a viable mechanism for the greater efficacy of MSN-SS-MXF when given by the i.m. vs. the i.v. route.

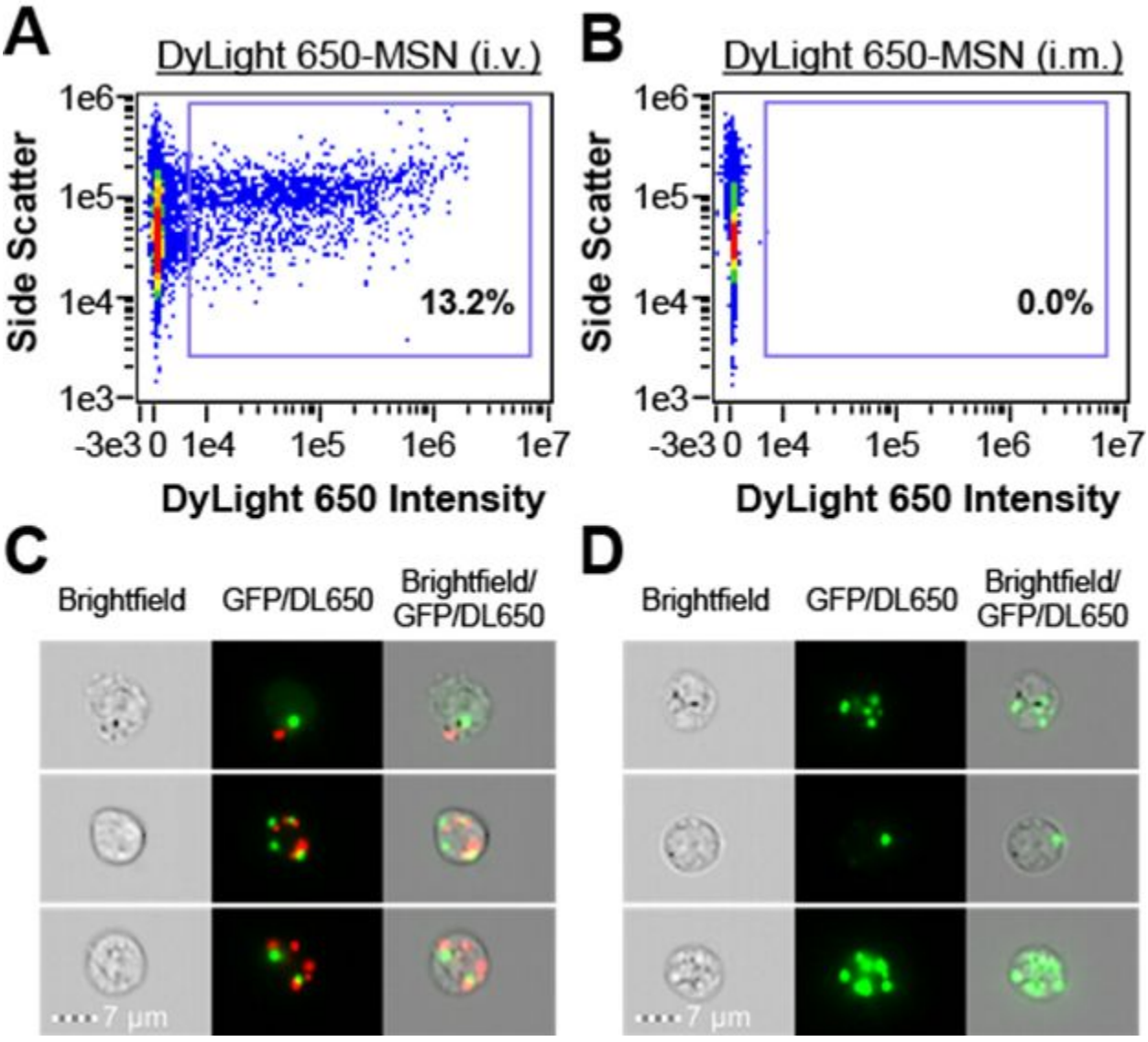

Fig. 4. DyLight 650-labeled MSNs are detected in lung cells after i.v. but not i.m. administration. (A, B) Imaging flow cytometry density plots of lung cells from mice infected with LVS-GFP were obtained one day after i.v. (A) or i.m. (B) administration of DyLight 650-labeled MSNs. (C) Images from (A) showing DyLight 650-positive lung cells that are also GFP-positive (i.e. infected with LVS-GFP). (D) Images from (B) showing DyLight 650-negative lung cells infected with LVS-GFP.

Pharmacokinetics of MXF in the blood following administration of free or MSN-SS-MXF by i.v. and i.m. routes

Because our ICP analysis and flow cytometry analysis both indicated that i.m. administered MSN-SS-MXF do not traffic to the lung, we used LC-MS to explore whether improved pharmacokinetics could account for the greater efficacy of i.m. vs. i.v. MSN-SS-MXF and the greater efficacy of MSN-SS-MXF vs. unencapsulated MXF. We administered a larger dose of MXF for these pharmacokinetic studies (280 μg MXF) because preliminary studies indicated that the lower doses (e.g. 50 μg) used in the efficacy studies provided too few data points above the limit of detection to adequately characterize and compare the PK profiles obtained with the different routes and formulations. Because the pharmacokinetics of fluoroquinolones in general[14,15] and MXF in particular[16,17] have been shown to be linear, our PK-PD indices determined with the 280 μg MXF dosing in our PK studies can be extrapolated to the lower 50 – 60 μg dosing used in our efficacy studies. The 280 μg MXF dose corresponds to 14 mg/kg and is not a high dose, as it is lower than the 100 mg/kg dose that has been used in other mouse infection models of tularemia[18] and tuberculosis.[19]

Mice were given equivalent amounts (280 μg) of free MXF or MSN-SS-MXF i.v. or i.m. and blood was obtained at sequential times thereafter for determination of MXF concentration by LC-MS (Figure 5). C_{max} values, defined as the highest concentrations measured as assessed from the time – concentration plot (Fig. 5), were highest for i.v. free MXF and i.v. MSN-SS-MXF, and lowest for i.m. MSN-SS-MXF (Table 3). The area under the curve (AUC) calculated by the linear trapezoidal method was lowest for the i.v. free MXF and similar for the i.v. MSN-SS-MXF, i.m. free MXF, and i.m. MSN-SS-MXF (Table 3). When calculated by the linear-up, log-down trapezoidal method,[20] i.m. MSN showed the greatest AUC, but the difference does not

appear to be great enough to account for its markedly greater efficacy (Table 3). On the other hand, the i.m. MSN-SS-MXF yielded a much longer half-life for MXF (6.9 hours) than i.v. MSN-SS-MXF (4.9 hours) and a considerably longer half-life than i.v. and i.m. free MXF (0.9 and 0.7 hours, respectively). Because of its much longer half-life, the time above the MIC for a 280 μg dose is longer following i.m. MSN-SS-MXF (24 hours) than i.v. MSN-SS-MXF (14 hours) and dramatically longer than for free MXF administered either i.v. or i.m. (5.1 and 5.5 hours, respectively). The same rank order of PK-PD indices are obtained assuming linear pharmacokinetics and extrapolating from the 280 μg dose used in our PK studies to the 50 μg dose used in our efficacy studies (Fig. 6 and Table 3). While all of the t>MIC values are shorter using the lower dose, the rank order remains the same, with i.m. MSN-SS-MXF being the longest (6.9 hours), i.v. MSN-SS-MXF the second longest (4.75 hours), and the i.m. and i.v. free MXF being the shortest (3.62 and 2.87 hours, respectively). The AUC/MIC and Cmax/MIC indices are proportionally decreased (Table 3). The t>MIC values predicted for the 50 μg dose of free MXF or MSN-SS-MXF given by the i.m. or i.v. routes correlate well with the observed lung CFU efficacy ratios, with a positive correlation coefficient ($R^2 = 0.992$, Fig. 6B). AUC/MIC has a positive but weaker correlation with efficacy ratio ($R^2 = 0.75$, Fig. 6C), and C_{max}/MIC shows a negative correlation with efficacy ratio (Fig. 6D).

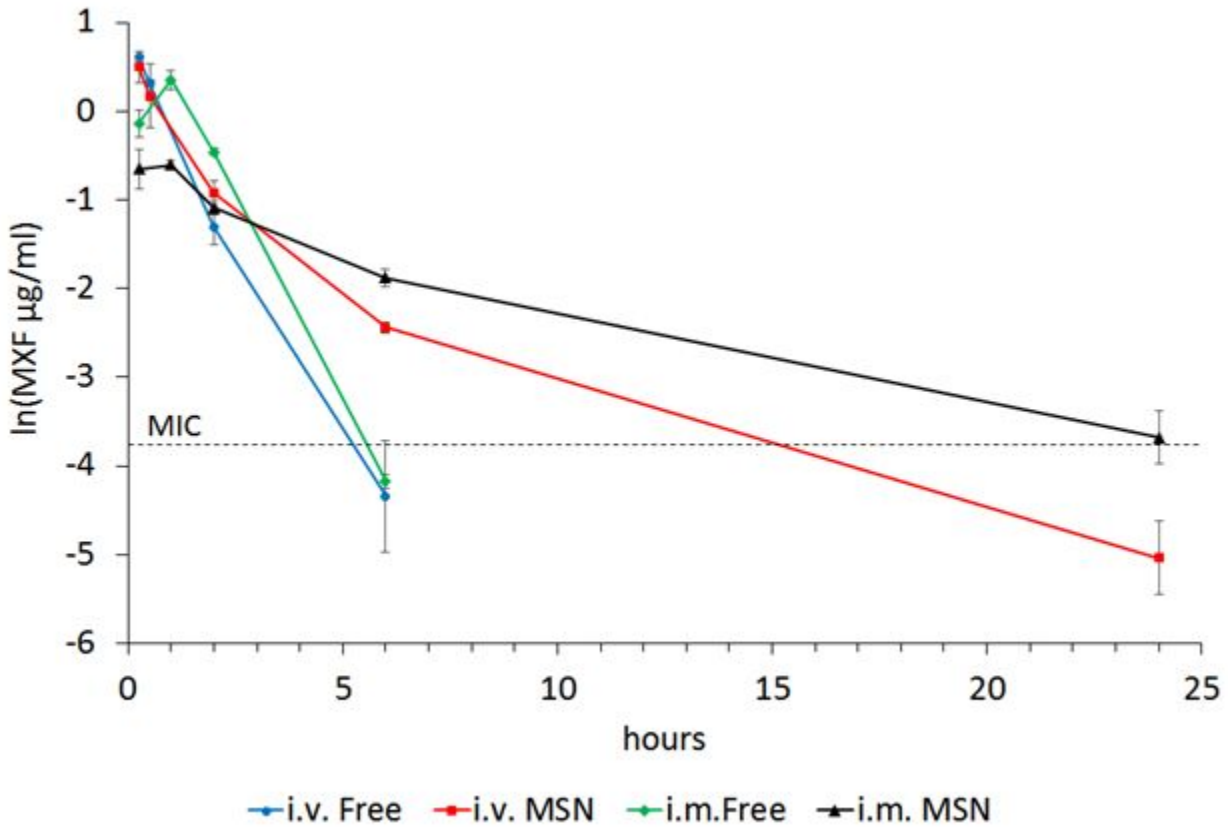

Fig. 5. Blood levels of MXF (plotted as natural log of µg/ml concentrations) after i.v. or i.m. administration of 0.28 mg of MXF either as free drug or as MSN-SS-MXF. The MXF MIC for LVS (0.025 µg/ml) is indicated with a dotted horizontal line. Blood MXF levels were below the limit of detection at time points greater than 6 hours after i.v. and i.m. administration of free MXF. Data are means ± SEM of determinations from 3 mice/data point.

Table 3. Pharmacokinetic parameters of MSN-SS-MXF and free MXF after i.v. and i.m. administration of a dose corresponding to 280 µg MXF and predicted values after a dose of 50 µg MXF.

Pharmacokinetic parameters and indices measured after a 280 µg dose of MXF	Free MXF		MSN-SS-MXF	
	i.v.	i.m.	i.v.	i.m.
K_{el} ($hours^{-1}$)	0.76	0.93	0.14	0.10
$t_{1/2}$ (hours)	0.91	0.74	4.95	6.93
C_{max} (µg/ml)	1.83	1.42	1.65	0.54
Linear trapezoidal $AUC_{0\text{-}48h}$ (µg·hours/ml)	2.54	3.42	3.56	3.49
Linear-up Log-down trapezoidal $AUC_{0\text{-}48h}$ (µg·hours/ml)	1.66	2.62	2.70	3.33
t>MIC (hours)	5.14	5.50	14.65	24.06
C_{max}/MIC	73.2	56.8	66	21.6
$AUC_{0\text{-}48h}$/MIC	66.4	104.8	108	133.2
Pharmacokinetic indices predicted after a 50 µg dose of MXF	**Free MXF**		**MSN-SS-MXF**	
	i.v.	i.m.	i.v.	i.m.
C_{max} (µg/ml)	0.33	0.25	0.29	0.10
Linear-up Log-down trapezoidal $AUC_{0\text{-}48h}$ (µg·hours/ml)	0.30	0.47	0.48	0.59
t>MIC (hours)	2.9	3.6	4.8	6.90
C_{max}/MIC	13.07	10.14	11.79	3.86
$AUC_{0\text{-}48h}$/MIC	11.86	18.71	19.29	23.79

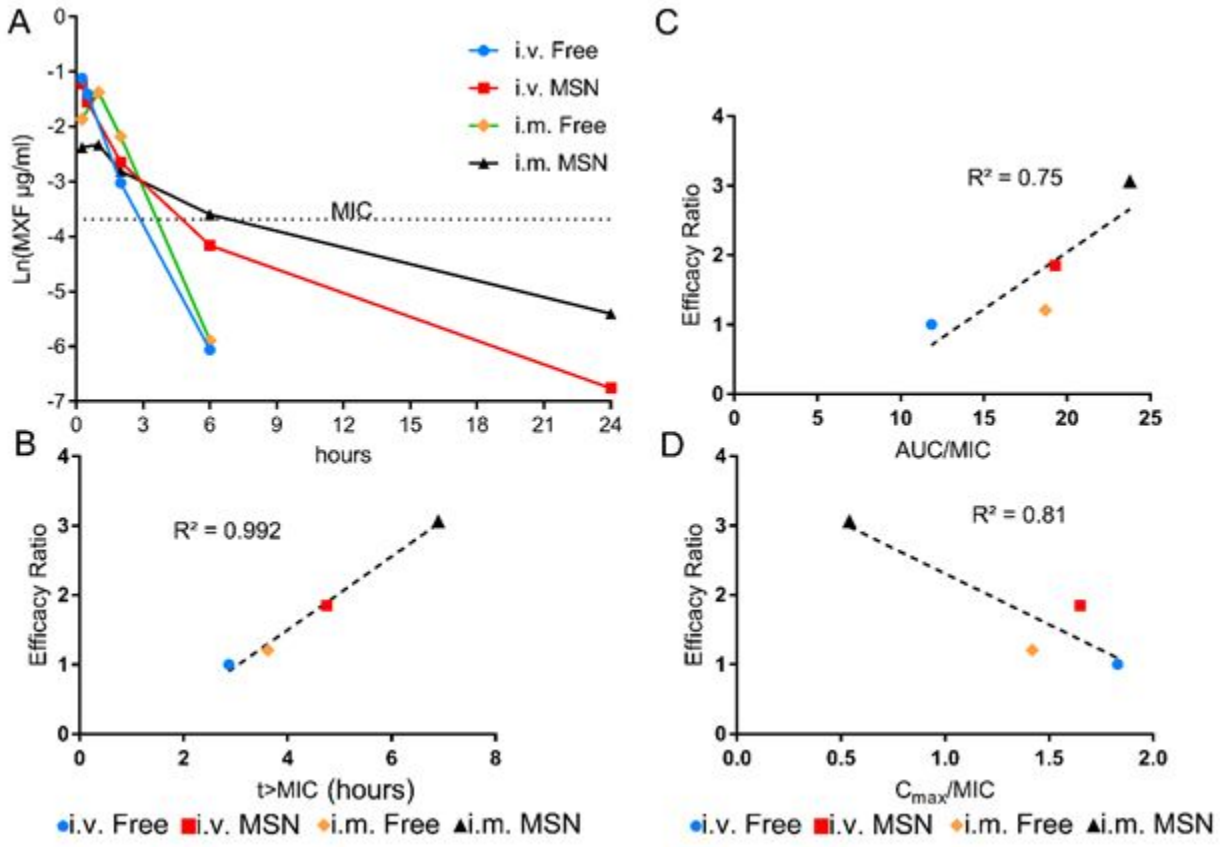

Fig. 6. Predicted blood levels of MXF after i.v. or i.m. administration of 50 µg of MXF either as free drug or as MSN-SS-MXF (A) and plots of pharmacokinetic indices vs. efficacy ratios (B - D). (A) Blood levels of MXF are calculated, assuming linear pharmacokinetics by extrapolation from Fig. 5 and plotted as natural log of µg/ml concentrations. The MXF MIC for LVS (0.025 µg/ml) is indicated with a dotted horizontal line. (B - D) Pharmacokinetic indices for t>MIC (B), AUC/MIC (C), and Cmax/MIC (D) from Table 3 are plotted on the x-axis and corresponding lung CFU efficacy ratios for the 50 µg dose of MXF (free MXF or MXF encapsulated in MSN-SS-MXF, delivered i.m. or i.v., relative to i.v. MXF, Table 2) are plotted on the y-axis. The coefficient of determination (R^2) between the efficacy ratio and each PK index is shown in each plot.

DISCUSSION

Research into antibiotic formulations, delivery platforms, and routes of administration has the potential to improve therapeutic index by increasing efficacy and decreasing toxicities. For example, in the case of fluoroquinolones, a liposomal formulation of ciprofloxacin delivered by the inhalational route has been shown to be much more effective than oral ciprofloxacin in a mouse model of pulmonary tularemia using the highly virulent Schu S4 strain of *F. tularensis*.[21] Liposomal and nanoparticle formulations each have advantages and disadvantages. While liposomal formulations are highly biocompatible and several have already received FDA approval for marketing, mesoporous silica nanoparticles have several potential advantages, including: 1) an extremely high drug loading capacity because of their high internal surface area,[22] 2) high physicochemical stability (e.g., they are not subject to phospholipid hydrolysis, phospholipid oxidation, and have negligible drug leakage), 3) a rigid structure that can be manufactured with different sizes and aspect ratios to optimize tissue penetration and cellular targeting properties,[23,24] 4) versatility in incorporation of design features to achieve stimulus controlled drug release from the pores of the MSN (e.g. in response to a change in redox potential, as in the current study),[1-4] and 5) facile modification of the surface of the MSN by attachment of ligands to promote specific cellular targeting.[1,22,25]

We have demonstrated in a mouse model of pneumonic tularemia that MXF formulated in redox-operated MSNs is markedly more efficacious than an equivalent amount of free drug and that this greater efficacy is further enhanced by administration of the MSNs i.m. vs. i.v. The greater efficacy of the MSN formulation is not attributable to enhanced delivery of the MSNs to infected cells or tissues, but instead to the markedly longer half-life of the MXF and the markedly longer duration that blood levels of MXF are above the MIC.

Three different pharmacokinetic parameters have been correlated with antibiotic treatment efficacy in various antibiotic-infection models: the ratio between peak blood level and MIC (Cmax/MIC); the AUC/MIC ratio; and time above MIC (t>MIC).[26-28] While administration of free MXF or MSN-SS-MXF i.v. leads to much higher Cmax than administration of MSN-SS-MXF i.m. (Fig. 5), the higher Cmax does not result in greater efficacy (Fig. 6D), suggesting that t>MIC or AUC/MIC is a more important factor in treatment efficacy in our model. While the linear trapezoidal method of AUC calculation is the standard method described in FDA guidance for bio-equivalence studies,[29] the linear-up/log-down trapezoidal AUC is likely a more accurate estimation of AUC as it corrects for the logarithmic as opposed to linear decline in MXF blood levels during the elimination phase.[20] Calculated by this method, the AUC/MIC ratio predicts the following efficacy ranking: i.m. MSN-SS-MXF > i.v. MSN-SS-MXF = i.m. free MXF > i.v. free MXF. On the other hand, t>MIC predicts an efficacy ranking of i.m. MSN-SS-MXF > i.v. MSN-SS-MXF > i.m. free MXF = i.v. free MXF (Table 3 and Fig. 6C). Table 2 data (excluding data for sites and doses at the limit of detection) show that the observed efficacy ranking matches the t>MIC prediction rather than the AUC/MIC prediction (Fig. 6B). This suggests that for our mouse model of tularemia, MXF efficacy is more time-dependent than concentration-dependent, i.e. concentrations substantially higher than the MIC do not provide more effective killing but concentrations above the MIC for a longer time do.

Both the antibiotic and the infectious agent are critical in determining which pharmacokinetic parameter is most important. In our system, i.m. administration of MXF in redox-operated snap top nanoparticles led to a dramatically prolonged half-life and prolonged t>MIC. While t>MIC was the best predictor of efficacy in our model of MXF treatment of pneumonic tularemia, in other infection-antibiotic models, such as the clinical response to

aminoglycoside therapy, the higher Cmax/MIC ratio provided by i.v. free drug may be more important to therapeutic efficacy. In addition, *F. tularensis* is exquisitely sensitive to fluoroquinolones, with an MIC(50) of 25 ng/ml for MXF in our studies, comparable to a published broth microdilution MIC(50) of 8 ng/ml for LVS[30] and 23 ng/ml for a *F. tularensis* subsp. *holarctica* clinical reference strain.[30] Other microbial pathogens have a higher MIC(50) for fluoroquinolones and would require higher doses than used in this study to achieve efficacy. For example, drug susceptible *M. tuberculosis* has an MIC(50) of 120 ng/ml[31] and the AUC/MIC ratio is the parameter found to be the best predictor of fluoroquinolone efficacy in a mouse model of tuberculosis.[32] We observed that nanoparticle encapsulated MXF also provided a higher AUC after i.m. than i.v. administration, and thus might also prove to be more effective for treatment of tuberculosis. Many infectious disease treatments are now shifting to drugs and formulations with longer half-lives as a means to improve treatment efficacy and to decrease the need for frequent dosing. For example, thrice weekly dosing of teichoplanin for treatment of out-patient bacterial infections,[33] once weekly treatment with dalbavancin for skin infections,[34] three times a week maintenance dosing of bedaquiline for TB treatment,[35] and once monthly dosing of cabotegravir/rilpivirine for HIV-1 infection.[36] Nanoparticle formulations such as ours and selection of dosing route (e.g. i.m. vs. i.v.) can be used to modulate the pharmacokinetic profile, increasing both t>MIC and AUC, to optimize treatment efficacy.

While we did not observe trafficking of our i.m. and s.c. delivered MSNs to lung, liver, or spleen, it is possible that different formulations of NPs or that an intradermal (i.d.) route of administration would have yielded more delivery of the MSNs to lung, liver, and spleen. In this regard, it is noteworthy that i.d. delivered pluronic-stabilized poly(propylene sulfide) NPs (<100 nm) have been shown to traffic through lymphatics to reach the blood and then be taken up by

mononuclear phagocytes in the spleen.[37] Indeed, the i.d. delivered NPs provided a 50% greater bioavailability in the blood than NPs delivered i.m.[37]

CONCLUSION

We have shown in a model of pulmonary tularemia that MXF encapsulated within redox-activated MSN is markedly more effective than free drug and that the i.m. route is more effective than the i.v. route. We have shown that this increased efficacy is not attributable to improved targeting, but instead to prolongation of the drug half-life and improved pharmacokinetics. In these studies, our MSN-SS-MXF have not been modified to include any specific targeting features, but instead rely on passive uptake. When given by the i.v. route, uptake is primarily into cells of the mononuclear phagocytic system in liver, spleen, and lung, which correlates well with the cells that are infected by *F. tularensis*. Indeed, our fluorescence flow cytometry analysis confirmed successful targeting of the nanoparticles administered by the i.v. route to infected cells in the lung. Nevertheless, we observed higher efficacy when the MSN-SS-MXF was given by i.m. and s.c. routes that did not lead to uptake of the nanoparticles by infected cells in these organs. While pharmacokinetic parameters proved more important than nanoparticle targeting in these studies, it is possible that incorporation of additional design features that further enhance nanoparticle targeting and delivery to lung tissue and to infected cells[38,39] would enhance the efficacy of the i.v. route of NP administration.

EXPERIMENTAL METHODS

Bacteria

F. tularensis LVS was acquired from the Centers for Disease Control and Prevention (Atlanta, GA). Frozen stocks of LVS and LVS expressing green fluorescent protein (LVS-GFP) were prepared from cultures on GC II agar with hemoglobin and IsoVitaleX enrichment (BD BBL) and pre-titered for use directly in animal experiments. *F. tularensis* subsp. *novicida* (*F. novicida*) was cultivated at 37°C with aeration in trypticase soy broth (BD BBL) supplemented with 0.2% cysteine (TSBC) for use in the bioassay for MXF.

MSN-SS-MXF and DyLight 650-labeled MSN

MSN-SS-MXF were prepared as previously described.[3] Briefly, cetyltrimethylammonium bromide (CTAB, 0.7 mmol) was mixed with NaOH (2 M, 1.7 mmol) in deionized water (120 ml). The solution was maintained at 80°C during dropwise addition of tetraethylorthosilicate (TEOS, 5.4 mmol). After 15 minutes, 3-(trihydroxysilyl) propyl methylphosphonate (HTMP, 0.5 mmol) was added to the mixture. The reaction temperature was maintained at 80°C for an additional 2 hours after which the MSNs were collected by centrifugation and washed three times with water and ethanol. The MSNs were modified with thiol groups by dispersing the MSNs and (3-mercaptopropyl) trimethoxysilane in dry toluene and refluxing under nitrogen atmosphere. CTAB was removed by suspending the MSNs (200 mg) in ethanol (80 ml) with the addition of concentrated HCl (10 ml) and refluxing for 1 hour, twice. The adamantane moiety was conjugated to the MSNs through formation of a disulfide bond. Typically, 1-adamantanethiol (17 mg, 0.1 mmole) and thiol group modified MSNs (100 mg) were mixed and suspended in anhydrous toluene (10 ml). The oxidizing reagent thiolcyanogen was prepared

separately by dispersing lead thiocyanate (800 mg) in 10 ml chloroform and titrating with bromine (200 µl) dissolved in chloroform (10 ml). The resultant mixture was filtered to obtain thiolcyanogen, which was slowly added to the MSN mixture at 4°C under nitrogen atmosphere. The adamantane-modified MSNs (MSN-SS-Ada) were washed thoroughly with toluene, ethanol and deionized water. MXF was loaded by suspending MSN-SS-Ada (10 mg) in 1 ml of 40 mM MXF in PBS and rotating overnight. β-cyclodextrin (40 mg) was then added to the solution as capping agent and the solution rotated for an additional 6 hours. The loaded MSNs (MSN-SS-MXF) were washed thoroughly prior to use.

Dylight 650-labeled MSNs were prepared by first mixing (3-aminopropyl) triethoxysilane (APTES, 0.2 mmol) with TEOS (4.5 mmol) and then adding the solution dropwise to the basic CTAB solution. After removal of CTAB, MSNs were suspended in DMF, and DyLight 650 NHS-Ester (500 µl) was added to allow covalent coupling to the amine groups grafted within the MSNs. After dye labeling, the particles were washed and processed as described above for disulfide snap-top modification.

Physicochemical characterization of the MSN

Transmission electron microscopy (TEM) images of MSN were obtained using a JEM1200-EX (JEOL) instrument (JEOL USA, Inc., Peabody, MA). Particle size and zeta potential were measured by ZetaSizer Nano (Malvern Instruments Ltd, Worcestershire, UK) with 50 µg/mL MSN dispersed in de-ionized water.

Measurement of MSN-SS-MXF release capacity

We used a modification of our previously described *F. novicida* bioassay [3] to determine the maximum amount of MXF released from particles. MXF released from MSN-SS-MXF in PBS or DMSO or acidified DMSO with and without 2-mercaptoethanol was measured by determining inhibition of *F. novicida* growth in TSBC.

Mouse model of pneumonic tularemia

Female BALB/c mice, age 8-9 weeks (Envigo), were acclimated for one week prior to infection with 4000 CFU (~6 x LD_{50}) of *F. tularensis* LVS i.n. Two mice were euthanized after infection (day 0) for determination of initial organ burden of *F. tularensis*. One day later (day 1), 3 additional mice were euthanized to determine the level of *F. tularensis* immediately before the start of treatment. Mice were treated with one of three doses of free MXF in PBS (3 mice/group for each dose) or one of two doses of MSN-SS-MXF (4 mice/group) i.v., s.c., or i.m. every other day (day 1, 3, and 5 for a total of three treatments). Sham-treated mice (3 mice/group) received an equal volume of PBS i.v. every other day on the same schedule. The mice were euthanized one day (day 6) after their third treatment, the organs harvested (lung, liver, and spleen), and the number of CFU determined by plating serial dilutions of organ homogenates on GCII chocolate agar plates containing sulfamethoxazole (40 μg/ml), trimethoprim (8 μg/ml), and erythromycin (50 μg/ml) to prevent growth of contaminants. Bacterial colonies were counted after incubation at 37°C for 4 days. All animal studies were approved by and conducted according to the procedures set forth by the UCLA Animal Research Committee (ARC # 1998-140).

Biodistribution of MSN-SS-MXF

BALB/c mice were fed a low silica diet and water throughout the experiment to optimize measurement of silica in organs. The mice were infected with *F. tularensis* LVS i.n. and administered either PBS i.v. or 0.28 mg MSN-SS-MXF i.v., s.c., or i.m. (4 mice/route) every other day for a total of 3 treatments, and euthanized 24 h later, as described above. Their organs were harvested, homogenized in PBS, digested with 67 - 70% HNO_3, evaporated, and reconstituted in a defined volume of 3-5 v/v% HNO_3 solution for analysis by ICP-OES (ICPE-9000, SHIMADZU, Japan).

Flow cytometry

BALB/c mice were acclimated for one week and infected with 4000 CFU LVS-GFP i.n. or left uninfected (negative control). Two days later, the infected mice were injected i.v. or i.m. with 1 mg of DyLight 650-labeled MSN or left untreated. Three days after infection with LVS-GFP, ~24 h after injection with DyLight 650-labeled MSNs, the mice were euthanized and their spleens and lungs harvested for analysis.

Single-cell suspensions of splenocytes were prepared by gently pressing the cells out of the spleen sac, lysing red blood cells with PharmLyse (BD Pharmingen), washing the cells, and filtering them through a 70-μm nylon cell strainer (Falcon). Single-cell suspensions of total lung cells were prepared by quickly chopping the lungs into small pieces with a scalpel and digesting for 1 h in 10 ml PBS containing 300 U/ml Collagenase type II (Worthington) and 0.15 mg/ml DNase I (Worthington) at 37°C with shaking (300 rpm). The lung cells were filtered through a 40-μm nylon cell strainer (Falcon), red blood cells lysed with PharmLyse, and the lung cells washed. Advanced RPMI 1640 (Invitrogen), supplemented with 2% heat-inactivated fetal

bovine serum, 2 mM l-alanyl-l-glutamine (Glutamax; Invitrogen), 10 mM HEPES buffer, 50 μM β-mercaptoethanol, and penicillin (100 IU/ml)-streptomycin (100 μg/ml), was used as the medium. Surface staining was performed in a 96-well V-bottom plate kept on ice. Lung and spleen cells (2 to 4 x 10^6 cells per well) were blocked with 4 μg anti-mouse CD16/32 (TruStain fcX, BioLegend), stained with 0.2 μg PE-labeled anti-mouse F4/80 (1:100 dilution) (BioLegend), washed, and fixed in 1% formaldehyde in PBS. Fixed cells were analyzed on an ImageStream Mark II Imaging Flow Cytometer and 30,000 events at 60x magnification were recorded for each sample gated by focus and aspect ratio vs. area parameters to obtain predominantly single cells. High quality single-cell images were obtained by gating events post acquisition with IDEAS® software version 4.0 (Amnis) using focus, aspect ratio vs. area, circularity, perimeter, diameter, and contrast parameters. This further refinement resulted in ~10,000 to 14,000 images for samples of lung cells and ~19,000 to 21,000 images for samples of spleen cells. Images with internalized LVS-GFP or internalized DyLight 650-labeled MSN were identified using intensity, max pixel, and internalization parameters. Samples from uninfected and/or untreated (i.e. not injected with MSN) mice were used as negative controls to determine where to draw the selection gates. Cells positive for F4/80 surface staining were gated using a side scatter vs. intensity plot; an unstained control was used to determine the location of the selection gate.

Drug dose-effect plots

The fraction of inhibition for samples treated with different doses of MXF was calculated using bacterial CFU in base-10 logarithm (log CFU) with the equation: Fraction of inhibition = 1 – (log CFU from sample treated with a known concentration of MXF or releasable MXF from

MSN-SS-MXF/log CFU from untreated sample). A median-effect plot[9,10] for MXF or MSN-SS-MXF was generated using MXF or MXF-equivalent (MSN) dose in base-10 logarithm as the X-axis and the fraction of surviving/killed bacteria in base-10 logarithm as the Y-axis.

Determination of MXF blood levels by LC-MS

MXF blood concentrations were determined by a modification of published methods.[40,41] Heparinized blood (0.1 ml) was collected by retro-orbital bleed at sequential times after administration of free MXF or MSN-SS-MXF i.v. or i.m. Ciprofloxacin (75 ng) was added to each sample as an internal standard and 9 volumes (0.9 ml) of acetonitrile were added and mixed thoroughly. The sample was stored overnight at 4°C, mixed again by vortex action, and insoluble material pelleted by centrifugation at 10,000*g* for 10 minutes. The supernate was transferred to a new tube and dried under vacuum. The dried material was resolubilized in 50 µl water and MXF was quantified by reverse-phase C18-LC-MS**.** LC analysis was performed on a Waters LCT Premier (TOF) Mass Spectrometer (positive electrospray ionization mode) with Acquity UPLC. Chromatographic separations were achieved by an Acquity UPLC BEH C18 column (1.7 µm, 2.1 x 50 mm). The mobile phase consisted of a water 0.3% formic acid/acetonitrile 0.3% formic acid mixture at a flow rate of 0.2 ml/min, with a sample injection volume of 5 µl. Linearity and recovery were assessed by spiking different MXF concentrations in mouse plasma with a ciprofloxacin internal standard. Calibration curves were fitted by a linear regression method through measurement of the ratios of peak areas corresponding to MXF and ciprofloxacin internal standard.

Statistics

Our previous studies using the *F. tularensis* LVS mouse model of tularemia and the same MSN-SS-MXF formulation showed differences between treatment group $\log_{10}$ CFU means of 3.3 standard deviations or larger.[3] Therefore, we chose a sample size of 3 mice per group to provide 80% power to confirm mean differences of 3.3 standard deviations or larger using the $p < 0.05$ significance criterion. We expanded the nanoparticle treatment groups to 4 mice per group for additional power to provide 80% power to confirm anticipated differences of 2.5 standard deviations or larger between the various nanoparticle treatment group means using the $p < 0.05$ significance criterion. Statistical analyses were performed using GraphPad Prism software (version 7.04). Means were compared across groups by two way analysis of variance (ANOVA) using the Tukey criteria to adjust p values for multiple comparisons. Comparisons of mean bacterial log CFU in the lung, liver, and spleen between mice treated with MSN-SS-MXF or an equivalent amount of free MXF were based on a logit transform linear dose response model for the log CFU results for free drug, not assuming parallel dose response relationships.[3] The adjusted mean for treatment with free drug was computed under this model, adjusted to the equivalent dose of MSN-SS-MXF, along with the corresponding p value for comparing the adjusted free drug mean to the MSN-SS-MXF mean. A p value of ≤ 0.05 was considered statistically significant.

Corresponding author

*E-mail: mhorwitz@mednet.ucla.edu

Notes

The authors declare no competing financial interest.

Acknowledgements

Funding: This work was supported by Defense Threat Reduction Agency Grant HDTRA1-13-1-0046 (to M.A.H. and J.I.Z.). We thank Saša Masleša-Galić, Susana Nava and Greg Khitrov (UCLA MIC) for excellent technical assistance. Flow cytometry was performed in the UCLA Jonsson Comprehensive Cancer Center (JCCC) and Center for AIDS Research Flow Cytometry Core Facility, which is supported by National Institutes of Health awards P30 CA016042 and 5P30 AI028697, and by the JCCC, the UCLA AIDS Institute, the David Geffen School of Medicine at UCLA, the UCLA Chancellor's Office, and the UCLA Vice Chancellor's Office of Research.

Abbreviations

ANOVA, analysis of variance; APTES, 3-aminopropyl triethozysilane; AUC, area under the curve; CFU, colony forming unit; C_{max}, maximum serum concentration; CTAB, cetyltrimethylammonium bromide; DLS, Dynamic light scattering; DMF, dimethylformamide; DMSO, dimethylsulfoxide; HTMP, 3-(trihydroxysilyl) propyl methylphosphonate; i.d., intradermal; i.m., intramuscular; i.n., intranasally; ICP-OES, inductively coupled plasma optical emission spectrometry; i.v., intravenous; K_{el}, elimination rate constant; LC, liquid

chromatography; LC-MS, liquid chromatography-mass spectrometry; $LD_{50,}$ dose causing 50% of untreated mice to die; LVS, Live Vaccine Strain; GFP, green fluorescence protein; MIC, minimum inhibitory concentration; MSN, mesoporous silica nanoparticle; MXF, moxifloxacin; MSN-SS-Ada, adamantane-modified MSN; MSN-SS-MXF, MSN-disulfide snaptop loaded with MXF; NP, nanoparticle; PBS, phosphate buffered saline; PD, pharmacodynamics; PK, pharmacokinetics; PLGA, poly-lactic-co-glycolic acid; R^2, correlation of determination; s.c., subcutaneous; SD, standard deviation; SEM, standard error of the mean; $t_{1/2}$, half-life; t>MIC, time above MIC; TEOS, tetraethylorthosilicate; TEM, transmission electron microscopy; TOF, time of flight; TSBC, trypticase soy broth supplemented with 0.2% cysteine; UPLC, ultra performance liquid chromatography; wt/wt %, weight/weight percentage

References

1. Li Z, Barnes JC, Bosoy A, Stoddart JF, and Zink JI (2012) Mesoporous silica nanoparticles in biomedical applications. *Chem Soc Rev 41*, 2590-2605 DOI 10.1039/c1cs15246g.
2. Coti KK, Belowich ME, Liong M, Ambrogio MW, Lau YA, Khatib HA, Zink JI, Khashab NM, and Stoddart JF (2009) Mechanised nanoparticles for drug delivery. *Nanoscale 1*, 16-39 DOI 10.1039/b9nr00162j.
3. Lee B-Y, Li Z, Clemens DL, Dillon BJ, Hwang AA, Zink JI, and Horwitz MA (2016) Redox-triggered release of moxifloxacin from mesoporous silica nanoparticles functionalized with disulfide snap-tops enhances efficacy against pneumonic tularemia in mice. *Small 12*, 3690-3702 DOI 10.1002/smll.201600892.
4. Ambrogio MW, Pecorelli TA, Patel K, Khashab NM, Trabolsi A, Khatib HA, Botros YY, Zink JI, and Stoddart JF (2010) Snap-top nanocarriers. *Org Lett 12*, 3304-3307 DOI 10.1021/ol101286a.
5. Li SD, and Huang L (2008) Pharmacokinetics and biodistribution of nanoparticles. *Mol Pharm 5*, 496-504 DOI 10.1021/mp800049w.
6. Hwang AA, Lee BY, Clemens DL, Dillon BJ, Zink JI, and Horwitz MA (2015) pH-Responsive Isoniazid-Loaded Nanoparticles Markedly Improve Tuberculosis Treatment in Mice. *Small 11*, 5065- 5078 DOI 10.1002/smll.201500937.
7. Clemens DL, Lee BY, Xue M, Thomas CR, Meng H, Ferris D, Nel AE, Zink JI, and Horwitz MA (2012) Targeted intracellular delivery of antituberculosis drugs to *Mycobacterium tuberculosis*-infected macrophages via functionalized mesoporous silica

nanoparticles. *Antimicrob Agents Chemother 56*, 2535-2545 DOI 10.1128/AAC.06049-11.

8. Fenaroli F, Westmoreland D, Benjaminsen J, Kolstad T, Skjeldal FM, Meijer AH, van der Vaart M, Ulanova L, Roos N, Nyström B, Hildahl J, and Griffiths G (2014) Nanoparticles as Drug Delivery System against Tuberculosis in Zebrafish Embryos: Direct Visualization and Treatment. *ACS Nano 8*, 7014-7026 DOI 10.1021/nn5019126.
9. Chou TC, and Talalay P (1984) Quantitative analysis of dose-effect relationships: the combined effects of multiple drugs or enzyme inhibitors. *Adv Enzyme Regul 22*, 27-55 DOI 10.1016/0065-2571(84)90007-4.
10. Chou TC (2006) Theoretical basis, experimental design, and computerized simulation of synergism and antagonism in drug combination studies. *Pharmacol Rev 58*, 621-681 DOI 10.1124/pr.58.3.10.
11. Sampah MES, Shen L, Jilek BL, and Siliciano RF (2011) Dose–response curve slope is a missing dimension in the analysis of HIV-1 drug resistance. *Proceedings of the National Academy of Sciences 108*, 7613 DOI 10.1073/pnas.1018360108.
12. García-Fuente A, Vázquez F, Viéitez JM, García Alonso FJ, Martín JI, and Ferrer J (2018) CISNE: An accurate description of dose-effect and synergism in combination therapies. *Scientific Reports 8*, 4964 DOI 10.1038/s41598-018-23321-6.
13. Lee JJ, and Kong M (2009) Confidence Intervals of Interaction Index for Assessing Multiple Drug Interaction. *Statistics in biopharmaceutical research 1*, 4-17 DOI 10.1198/sbr.2009.0001.
14. Scaglione F, Mouton JW, Mattina R, and Fraschini F (2003) Pharmacodynamics of levofloxacin and ciprofloxacin in a murine pneumonia model: peak concentration/MIC

versus area under the curve/MIC ratios. *Antimicrob Agents Chemother 47*, 2749-2755 DOI 10.1128/AAC.47.9.2749-2755.2003.

15. Lode H, Borner K, and Koeppe P (1998) Pharmacodynamics of fluoroquinolones. *Clin Infect Dis 27*, 33-39 DOI 10.1086/514623.

16. Stass H, Dalhoff A, Kubitza D, and Schuhly U (1998) Pharmacokinetics, safety, and tolerability of ascending single doses of moxifloxacin, a new 8-methoxy quinolone, administered to healthy subjects. *Antimicrob Agents Chemother 42*, 2060-2065 DOI 10.1128/AAC.42.8.2060.

17. Sullivan JT, Woodruff M, Lettieri J, Agarwal V, Krol GJ, Leese PT, Watson S, and Heller AH (1999) Pharmacokinetics of a once-daily oral dose of moxifloxacin (Bay 12-8039), a new enantiomerically pure 8-methoxy quinolone. *Antimicrob Agents Chemother 43*, 2793-2797 DOI 10.1128/AAC.43.11.2793.

18. Piercy T, Steward J, Lever MS, and Brooks TJG (2005) In vivo efficacy of fluoroquinolones against systemic tularaemia infection in mice. *Journal of Antimicrobial Chemotherapy 56*, 1069-1073 DOI 10.1093/jac/dki359.

19. Yoshimatsu T, Nuermberger E, Tyagi S, Chaisson R, Bishai W, and Grosset J (2002) Bactericidal activity of increasing daily and weekly doses of moxifloxacin in murine tuberculosis. *Antimicrobial Agents and Chemotherapy 46*, 1875-1879 DOI 10.1128/AAC.46.6.1875-1879.2002.

20. Chiou WL (1978) Critical evaluation of the potential error in pharmacokinetic studies of using the linear trapezoidal rule method for the calculation of the area under the plasma level--time curve. *J Pharmacokinet Biopharm 6*, 539-546 DOI 10.1007/BF01062108.

21. Hamblin KA, Armstrong SJ, Barnes KB, Davies C, Wong JP, Blanchard JD, Harding SV, Simpson AJH, and Atkins HS (2014) Liposome encapsulation of ciprofloxacin improves protection against highly virulent *Francisella tularensis* Strain Schu S4. *Antimicrobial Agents and Chemotherapy 58*, 3053 DOI 10.1128/AAC.02555-13.

22. Tarn D, Ashley CE, Xue M, Carnes EC, Zink JI, and Brinker CJ (2013) Mesoporous silica nanoparticle nanocarriers: biofunctionality and biocompatibility. *Acc Chem Res 46*, 792–801 DOI 10.1021/ar3000986.

23. Meng H, Yang S, Li Z, Xia T, Chen J, Ji Z, Zhang H, Wang X, Lin S, Huang C, Zhou ZH, Zink JI, and Nel AE (2011) Aspect ratio determines the quantity of mesoporous silica nanoparticle uptake by a small GTPase-dependent macropinocytosis mechanism. *ACS Nano 5*, 4434-4447 DOI 10.1021/nn103344k.

24. Huang X, Teng X, Chen D, Tang F, and He J (2010) The effect of the shape of mesoporous silica nanoparticles on cellular uptake and cell function. *Biomaterials 31*, 438-448 DOI 10.1016/j.biomaterials.2009.09.060.

25. Liong M, Angelos S, Choi E, Patel K, Stoddart JF, and Zink JI (2009) Mesostructured multifunctional nanoparticles for imaging and drug delivery. *Journal of Materials Chemistry 19*, 6251-6257 DOI 10.1039/B902462J.

26. Wright DH, Brown GH, Peterson ML, and Rotschafer JC (2000) Application of fluoroquinolone pharmacodynamics. *J Antimicrob Chemother 46*, 669-683 DOI 10.1093/jac/46.5.669.

27. Moore RD, Lietman PS, and Smith CR (1987) Clinical response to aminoglycoside therapy: importance of the ratio of peak concentration to minimal inhibitory concentration. *J Infect Dis 155*, 93-99 DOI 10.1093/infdis/155.1.93.

28. Schentag JJ, Nix DE, and Adelman MH (1991) Mathematical examination of dual individualization principles (I): Relationships between AUC above MIC and area under the inhibitory curve for cefmenoxime, ciprofloxacin, and tobramycin. *DICP 25*, 1050-1057 DOI 10.1177/106002809102501003.

29. FDA (2006) Guidance for Industry: Bioequivalence Guidance; Docket No. 94D-0401; https://www.fda.gov/downloads/AnimalVeterinary/GuidanceComplianceEnforcement/GuidanceforIndustry/ucm052363.pdf, accessed Nov. 23, 2018.

30. Yesilyurt M, Kilic S, Celebi B, Celik M, Gul S, Erdogan F, and Ozel G (2011) Antimicrobial susceptibilities of Francisella tularensis subsp. holarctica strains isolated from humans in the Central Anatolia region of Turkey. *J Antimicrob Chemother 66*, 2588-2592 DOI 10.1093/jac/dkr338.

31. Gillespie SH, and Billington O (1999) Activity of moxifloxacin against mycobacteria. *J Antimicrob Chemother 44*, 393-395 DOI 10.1093/jac/44.3.393.

32. Shandil RK, Jayaram R, Kaur P, Gaonkar S, Suresh BL, Mahesh BN, Jayashree R, Nandi V, Bharath S, and Balasubramanian V (2007) Moxifloxacin, ofloxacin, sparfloxacin, and ciprofloxacin against Mycobacterium tuberculosis: evaluation of in vitro and pharmacodynamic indices that best predict in vivo efficacy. *Antimicrob Agents Chemother 51*, 576-582 DOI 10.1128/AAC.00414-06.

33. Lamont E, Seaton RA, Macpherson M, Semple L, Bell E, and Thomson AH (2009) Development of teicoplanin dosage guidelines for patients treated within an outpatient parenteral antibiotic therapy (OPAT) programme. *J Antimicrob Chemother 64*, 181-187 DOI 10.1093/jac/dkp147.

34. Boucher HW, Wilcox M, Talbot GH, Puttagunta S, Das AF, and Dunne MW (2014) Once-weekly dalbavancin versus daily conventional therapy for skin infection. *N Engl J Med 370*, 2169-2179 DOI 10.1056/NEJMoa1310480.

35. FDA (2013) Sirturo prescribing information; https://www.accessdata.fda.gov/drugsatfda_docs/label/2013/204384s002lbl.pdf, accessed Nov. 23, 2018.

36. Margolis DA, Gonzalez-Garcia J, Stellbrink HJ, Eron JJ, Yazdanpanah Y, Podzamczer D, Lutz T, Angel JB, Richmond GJ, Clotet B, Gutierrez F, Sloan L, Clair MS, Murray M, Ford SL, Mrus J, Patel P, Crauwels H, Griffith SK, Sutton KC, Dorey D, Smith KY, Williams PE, and Spreen WR (2017) Long-acting intramuscular cabotegravir and rilpivirine in adults with HIV-1 infection (LATTE-2): 96-week results of a randomised, open-label, phase 2b, non-inferiority trial. *Lancet 390*, 1499-1510 DOI 10.1016/S0140-6736(17)31917-7.

37. Kourtis IC, Hirosue S, de Titta A, Kontos S, Stegmann T, Hubbell JA, and Swartz MA (2013) Peripherally administered nanoparticles target monocytic myeloid cells, secondary lymphoid organs and tumors in mice. *PLoS One 8*, e61646 DOI 10.1371/journal.pone.0061646.

38. Friedman AD, Claypool SE, and Liu R (2013) The smart targeting of nanoparticles. *Curr Pharm Des 19*, 6315-6329 DOI 10.2174/13816128113199990375.

39. Oh P, Borgstrom P, Witkiewicz H, Li Y, Borgstrom BJ, Chrastina A, Iwata K, Zinn KR, Baldwin R, Testa JE, and Schnitzer JE (2007) Live dynamic imaging of caveolae pumping targeted antibody rapidly and specifically across endothelium in the lung. *Nat Biotechnol 25*, 327-337 DOI 10.1038/nbt1292.

40. Lee SJ, Desta KT, Eum SY, Dartois V, Cho SN, Bae DW, and Shin SC (2016) Development and validation of LC-ESI-MS/MS method for analysis of moxifloxacin and levofloxacin in serum of multidrug-resistant tuberculosis patients: Potential application as therapeutic drug monitoring tool in medical diagnosis. *J Chromatogr B Analyt Technol Biomed Life Sci 1009-1010*, 138-143 DOI 10.1016/j.jchromb.2015.11.058.

41. Respaud R, Grayo S, Singlas E, Dubouch S, Le Monnier A, and Lott MC (2012) High-performance liquid chromatography assay for moxifloxacin in brain tissue and plasma: validation in a pharmacokinetic study in a murine model of cerebral listeriosis. *J Anal Methods Chem 2012*, 436349 DOI 10.1155/2012/436349.

Table of Contents/Abstract Graphic

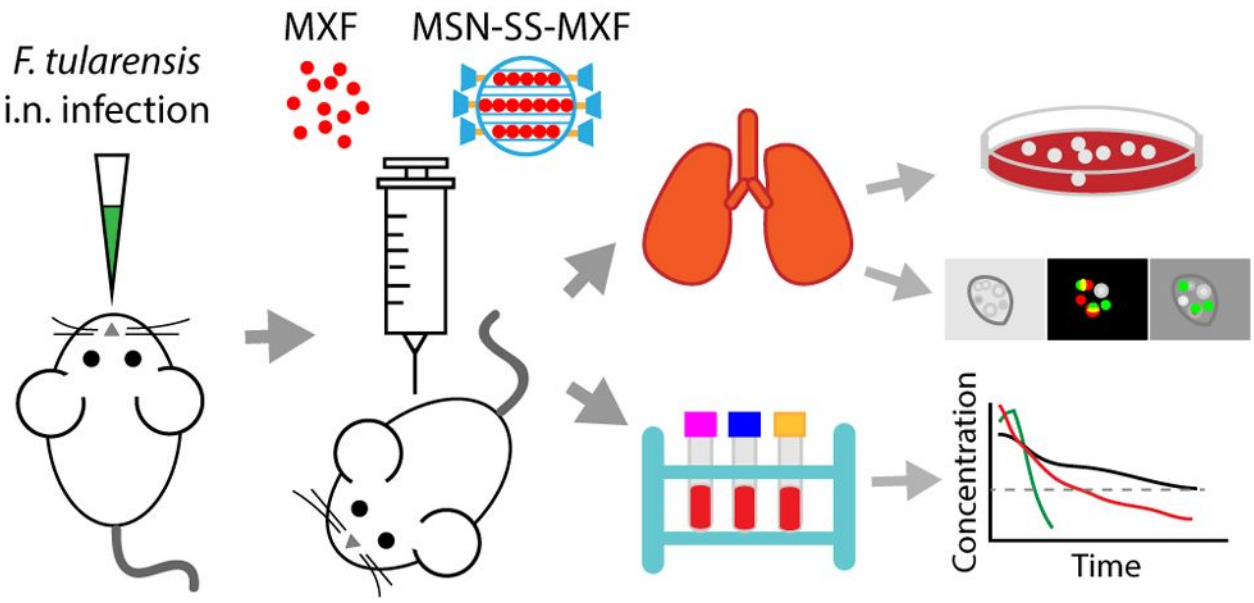

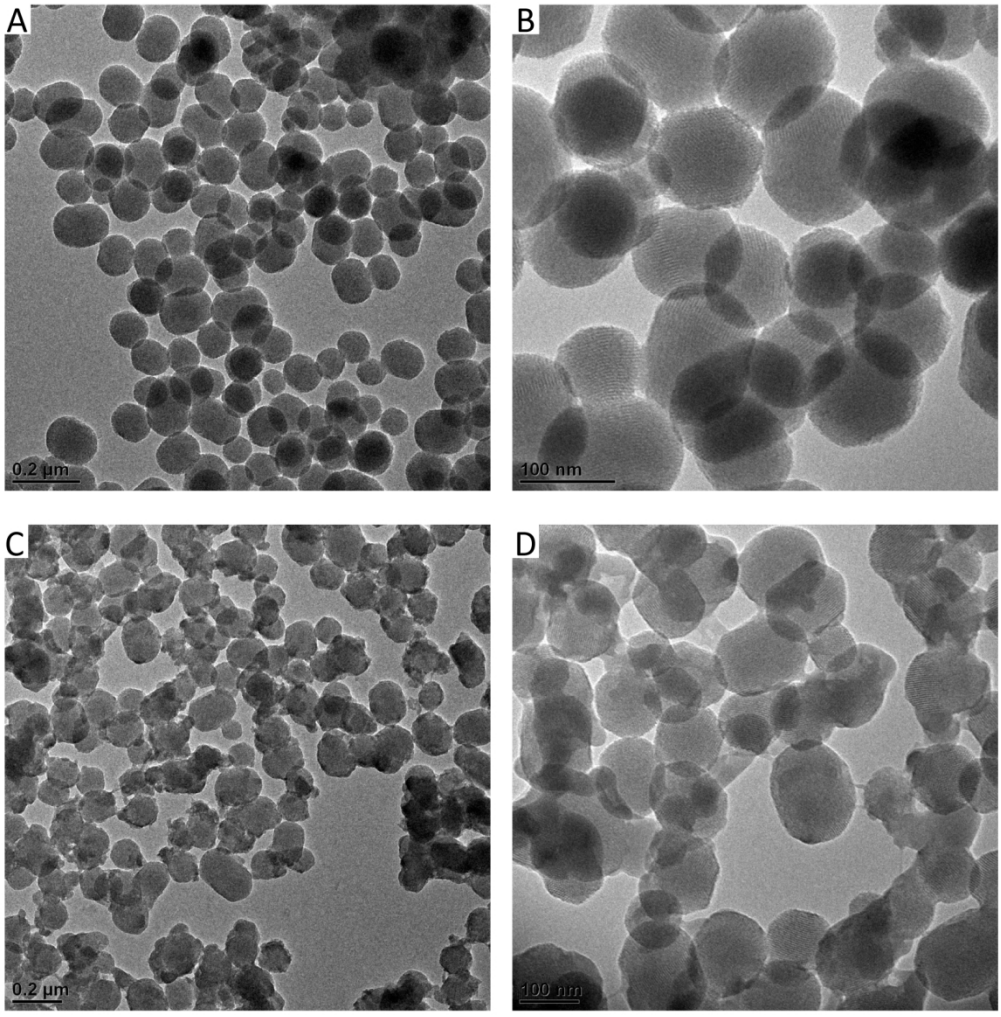

Fig. 1. TEM image of MSN before (A - B) and after (C - D) surface modification to incorporate redox-operated snap-top nanovalves. Size bars (A, C) 0.2 µm; (B, D) 100 nm

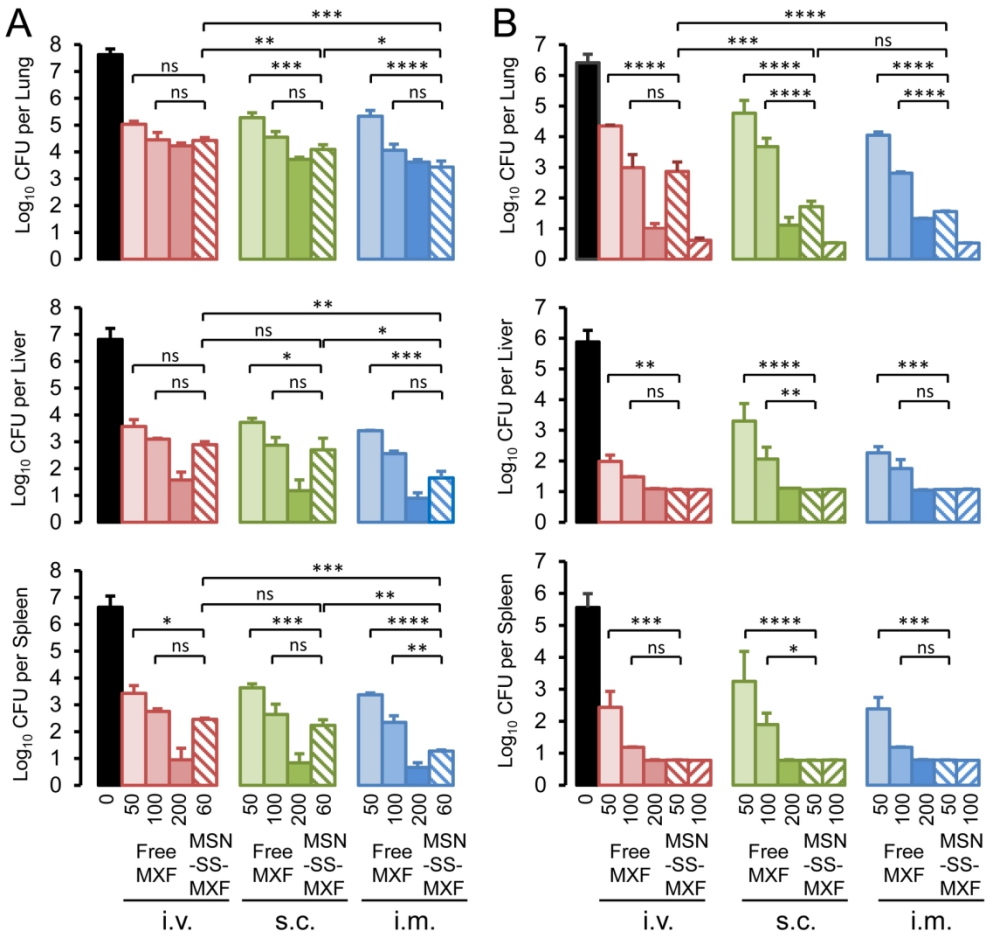

Fig. 2. Efficacy of MSN-SS-MXF and free MXF administered i.v., s.c., or i.m. in two independent experiments. BALB/c mice were infected with *F. tularensis* LVS i.n. at day 0. Mice were treated on day 1, 3, and 5 with free MXF (n = 3 mice/group) or MSN-SS-MXF (n = 4 mice/group) at the dose and route of administration indicated. Control mice were sham-treated with PBS i.v. Doses of MSN-SS-MXF indicated in the first (A) and second (B) experiments were the amount of free MXF-equivalent delivered. Bacterial burdens in the lung (top panel), liver (middle panel), and spleen (bottom panel) were determined one day after the last treatment on day 6. Data are mean ± SEM. Treatment efficacy between groups was analyzed using two-way ANOVA with Tukey's multiple comparisons test. ****, $p < 0.0001$; ***, $p < 0.001$; **, $p < 0.01$; *, $p < 0.05$; ns, not significant

160x152mm (300 x 300 DPI)

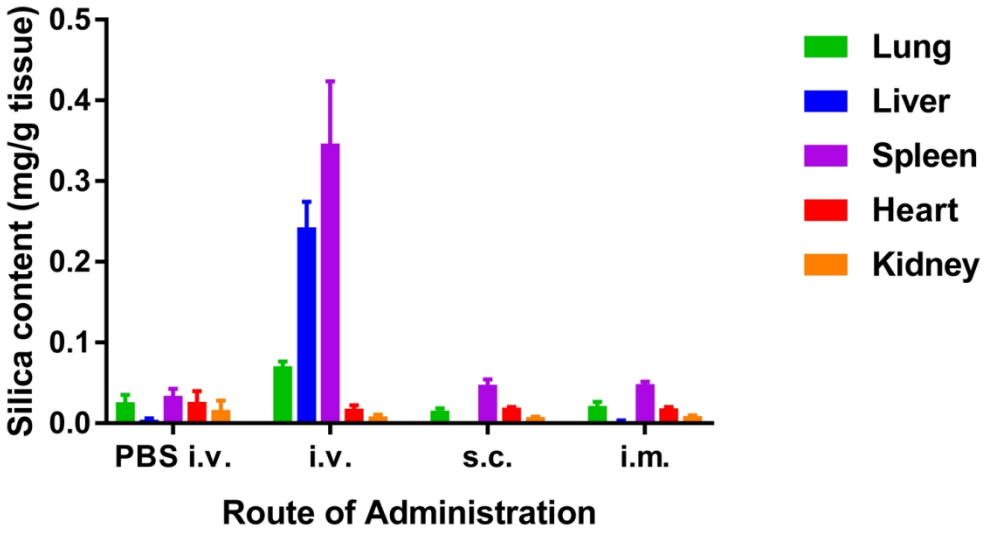

Fig. 3. Organ biodistribution of silica. The amount of silica in organs from *F. tularensis* LVS infected mice was determined after administration of MSN-SS-MXF via the route indicated. Data are mean ± SD of 3 mice in the PBS i.v. group and 4 mice each in the MSN-SS-MXF i.v., s.c., and i.m. groups.

125x69mm (300 x 300 DPI)

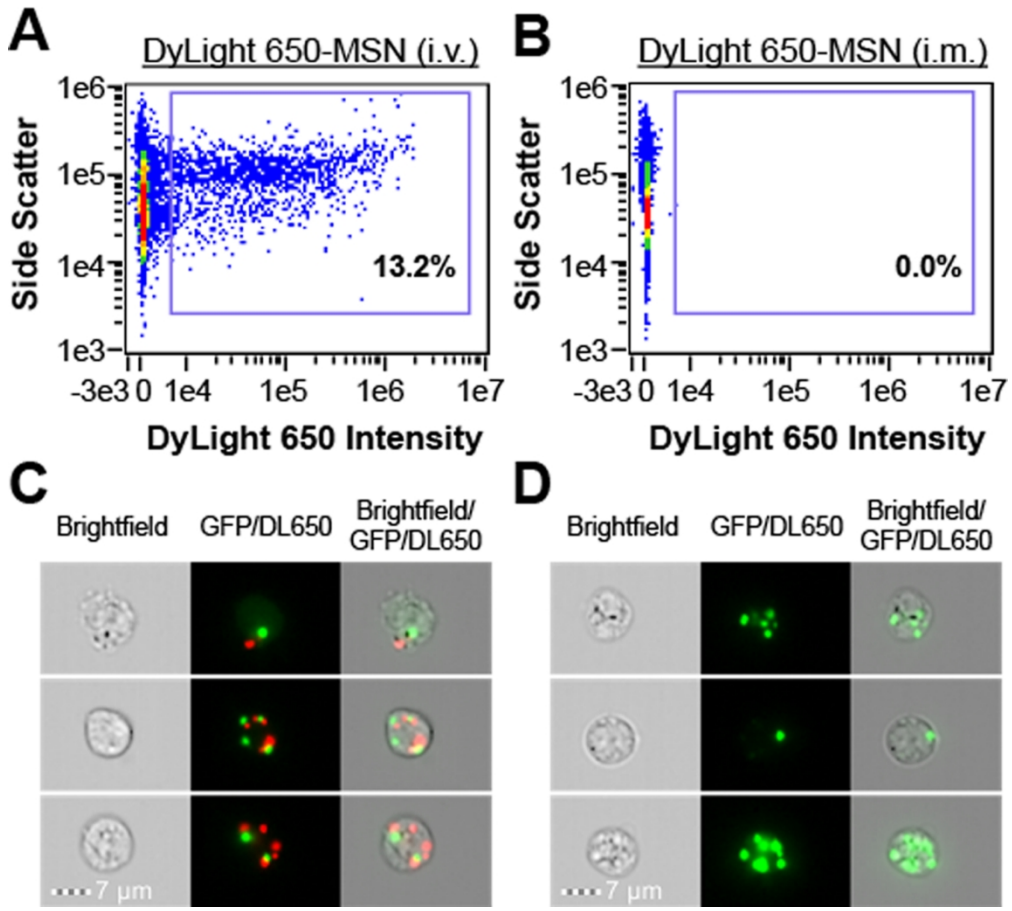

Fig. 4. DyLight 650-labeled MSNs are detected in lung cells after i.v. but not i.m. administration. (A, B) Imaging flow cytometry density plots of lung cells from mice infected with LVS-GFP were obtained one day after i.v. (A) or i.m. (B) administration of DyLight 650-labeled MSNs. (C) Images from (A) showing DyLight 650-positive lung cells that are also GFP-positive (i.e. infected with LVS-GFP). (D) Images from (B) showing DyLight 650-negative lung cells infected with LVS-GFP.

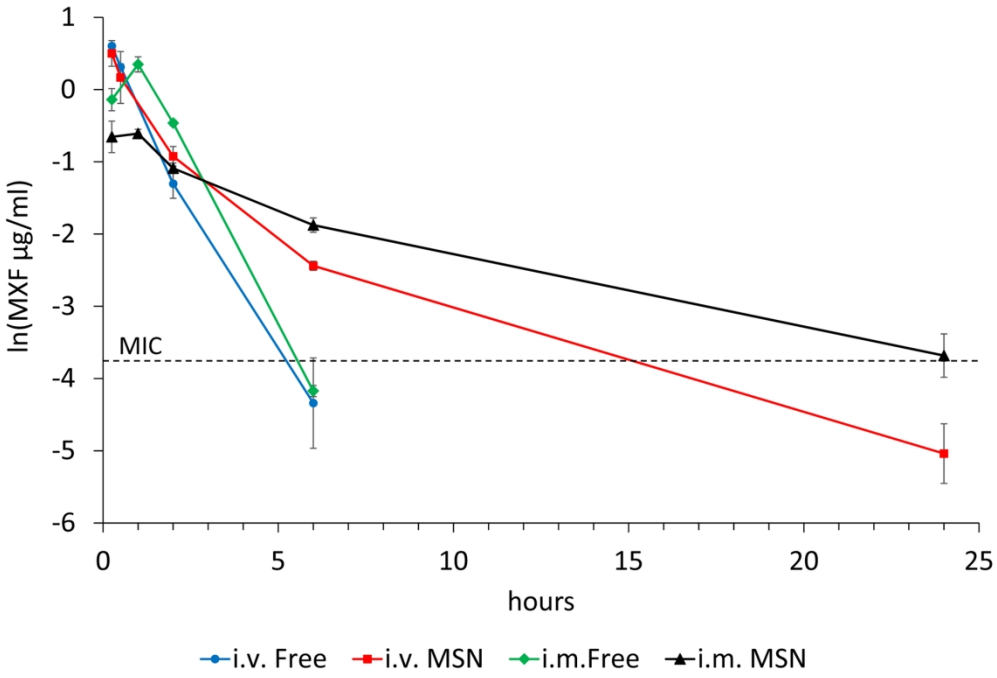

Fig. 5. Blood levels of MXF (plotted as natural log of µg/ml concentrations) after i.v. or i.m. administration of 0.28 mg of MXF either as free drug or as MSN-SS-MXF. The MXF MIC for LVS (0.025 µg/ml) is indicated with a dotted horizontal line. Blood MXF levels were below the limit of detection at time points greater than 6 hours after i.v. and i.m. administration of free MXF. Data are means ± SEM of determinations from 3 mice/data point.

177x121mm (300 x 300 DPI)

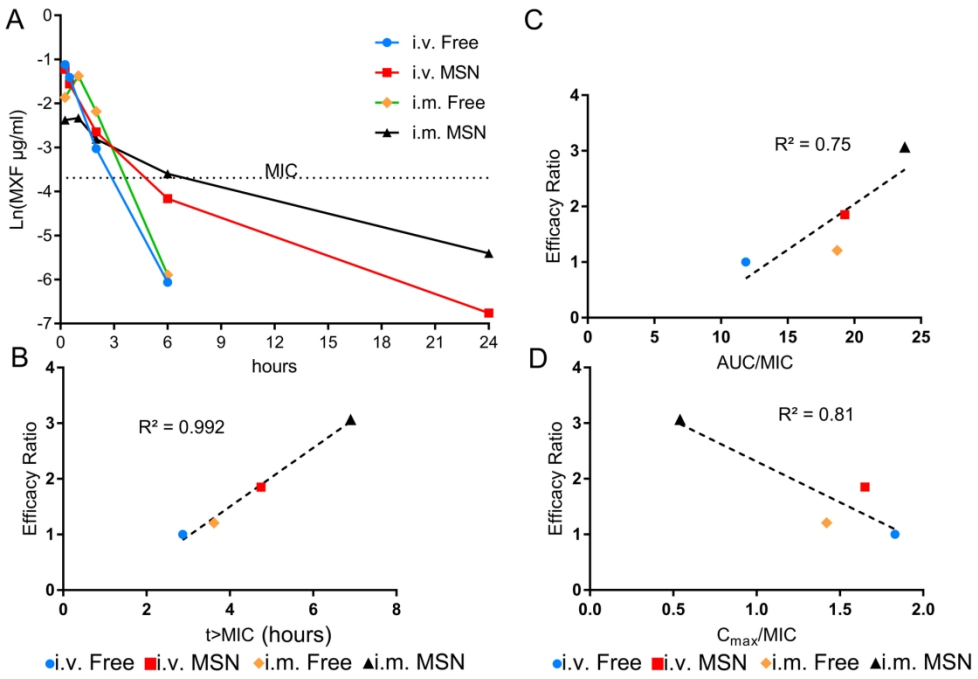

Fig. 6. Predicted blood levels of MXF after i.v. or i.m. administration of 50 µg of MXF either as free drug or as MSN-SS-MXF (A) and plots of pharmacokinetic indices vs. efficacy ratios (B - D). (A) Blood levels of MXF are calculated, assuming linear pharmacokinetics by extrapolation from Fig. 5 and plotted as natural log of µg/ml concentrations. The MXF MIC for LVS (0.025 µg/ml) is indicated with a dotted horizontal line. (B - D) Pharmacokinetic indices for t>MIC (B), AUC/MIC (C), and Cmax/MIC (D) from Table 3 are plotted on the x-axis and corresponding lung CFU efficacy ratios for the 50 µg dose of MXF (free MXF or MXF encapsulated in MSN-SS-MXF, delivered i.m. or i.v., relative to i.v. MXF, Table 2) are plotted on the y-axis. The coefficient of determination (R2) between the efficacy ratio and each PK index is shown in each plot.

177x124mm (300 x 300 DPI)

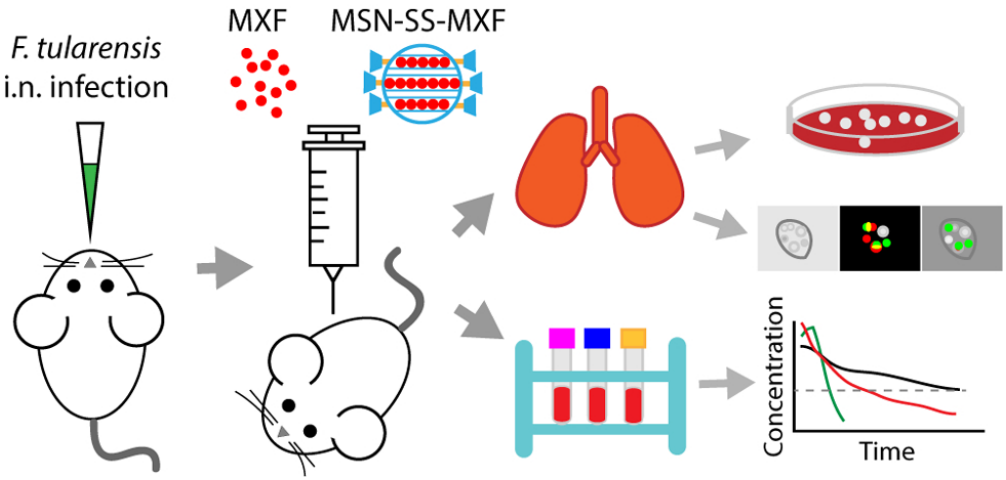

TOC Graphic Abstract